CrossMark

ORIGINAL PAPER

Subtropical/polar jet influence on Plains and Southeast tornado outbreaks

Robert T. Kelnosky[1] · Gregory J. Tripoli[1] · Jonathan E. Martin[1]

Abstract While extensive research consideration has been given to the Northern Hemispheric polar (PJ) and subtropical jet (STJ) streams, there have been fewer climatological studies relating these two jet types to tornado outbreaks. This study examines tornado outbreaks in two regions with substantial tornado risk, Plains Tornado Alley (PTA) and Southeast Tornado Alley (STA), and classifies the jet streak types associated with the outbreaks. Utilizing the Storm Prediction Center (SPC) tornado database and an objective jet identification scheme created from NCEP/NCAR Reanalysis 1 data, jet streaks were identified as STJ, PJ, merged (identified as STJ and PJ), superposed, or unidentified for a 30-year period between 1984 and 2013. Tornado outbreaks were categorized into different types based on these jet streak types. Results revealed STJ and PJ tornado outbreaks compose the majority of tornado outbreaks, as well as the most intense outbreaks, in both PTA and STA. STJ tornado outbreaks were found to be more common in PTA than in STA, while PJ outbreaks were more common in STA than in PTA. The study concludes by considering how a coupled jet structure may be important for tornado outbreaks.

✉ Robert T. Kelnosky
    kelnosky@wisc.edu

[1] Department of Atmospheric and Oceanic Sciences, University of Wisconsin-Madison, 1255 W. Dayton St., Madison, WI 53706, USA

🖄 Springer

1 Introduction

The subtropical (STJ) and polar jet (PJ) streams provide a number of well-known and vital ingredients for organized convective modes, including convective instability, dynamic lifting, and vertical wind shear (Beebe and Bates 1955; Lee and Galway 1956, 1958; Palmén and Newton 1969; McNulty 1978; Hales 1979; Uccellini and Johnson 1979; Bluestein and Thomas 1984). The PJ is associated with transverse vertical circulations extending to the surface, and strong low- and middle-tropospheric horizontal baroclinicity (Reiter 1963). Meanwhile, the STJ is associated with weaker horizontal baroclinicity that may extend to the surface.

Upper-level jet streaks have long been known to be associated with environments supportive of severe deep moist convection and tornadoes. Fawbush et al. (1951) observed one of the synoptic conditions conducive to tornado development is the intersection of the vertical projection of the axis of an upper-level jet with the axis of a low-level moisture ridge. This moisture ridge results from, and is aligned along, a low-level jet (Beebe and Bates 1955). With the use of the Riehl et al. (1952) four-quadrant model, Beebe and Bates (1955) proposed various configurations of an upper-level jet at 500 hPa intersecting a low-level jet at 850 hPa to create the necessary upper upward motion (associated with upper-level divergence/low-level convergence) to release convective instability. Lee and Galway (1956, 1958) used Beebe and Bates' findings to relate horizontal wind maxima and their associated areas of horizontal divergence to tornado occurrence in papers directly related to operational severe weather forecasting. Whitney (1977), relating satellite depictions of severe storms to the positions of the PJ and STJ, found severe storms were sharply inhibited equatorward of the STJ, and severe storms, particularly tornadoes, tended to occur between the STJ and PJ and ahead of a surface front. Emphasizing the 300-hPa level instead of the often considered 500-hPa level, McNulty (1978) suggested the divergent quadrant of the wind maxima at the 300–200-hPa layer may be used in combination with low-level moisture, instability, and convergence to define areas of severe thunderstorm and tornado occurrence. McNulty also noted the intersection of the upper- and lower-level jets is not necessary to produce severe storms, instead finding a horizontal separation of less than 900 km sufficient. Hales (1979) noted how little correlation was there between vorticity advection at 250 hPa and severe storm occurrence, and suggested considering 250-hPa horizontal wind shear in conjunction with 250-hPa vorticity advection to help recognize areas with a potential of severe weather occurrence. Uccellini and Johnson (1979) suggested a low-level jet can form as a result of the isallobaric contribution to the ageostrophic wind and demonstrated the low-level jet is linked to the transverse circulation of the jet exit region of an upper-level jet streak. The transverse circulation of the jet exit region is associated with storm formation and sustenance, which was explored in a case study with an unusually strong upper-level jet streak by Bluestein and Thomas (1984).

There have been more recent studies focusing on relating jet quadrants to tornado occurrence. Neglecting the distinction between STJ and PJ, Rose et al. (2004) utilized the four-quadrant jet streak model and found a higher percentage of F/EF1(Fujita/Enhanced Fujita) or stronger tornadoes occurred in the exit region of jet streaks, with the left jet exit region being more dominant. By including F/EF0 tornadoes and curved jet streaks that Rose et al. (2004) chose to disregard, Clark et al. (2009) found tornadoes were more evenly distributed over jet regions. Rose et al. (2004) also found a greater tornado occurrence rate in the left-exit and right-entrance regions for tornado outbreak day in which six or greater F/EF1 tornadoes occurred compared to non-outbreak days. Forbes (2006) furthered these results finding the right-entrance region is not as important for high-impact tornado

outbreaks (determined via the Forbes impact index), but instead the exit region of an upper-level jet streak is in general more significant. The Forbes impact index is a 100-point scale that utilizes eleven tornado outbreak attributes to numerically describe the impact of a tornado outbreak.

These climatology studies did not address any geographical regional differences, which may have additional value for forecasters. Certainly, the climatology of tornado frequency differs among the Midwest or Great Plains Tornado Alley (hereafter PTA) and Southeast Tornado Alley (STA) (e.g., Kelly et al. 1978; Concannon et al. 2000; Brooks et al. 2003; Gagan et al. 2010). PTA is a region commonly thought of as "classic" or "traditional" tornado alley, while STA is a region in the southeastern USA that has garnered more attention in recent years due to its annual high number of significant tornadoes and high number of tornado-related fatalities (e.g., Ashley 2007; Ashley et al. 2008). Topography between the two alleys also differs; STA generally is lower in elevation, has more rugged and hilly terrain, and has more vegetation than PTA. The more variable terrain in STA may cause a number of effects on tornadogenesis and tornado tracking that differs from the flat terrain of PTA, but because the understanding of how terrain and vegetation affect tornadogenesis and maintenance remains poorly understood, it will be neglected here.

Kelly et al. (1978) used a tornado dataset extensively reviewed for accuracy, although limitations to the dataset existed. This likely introduced biases to the tornado dataset, which eventually became the Storm Prediction Center (SPC) tornado database (Schaefer and Edwards 1999). Kelly et al. (1978) reported the highest tornado frequency during 1950–1975 over the Great Plains. Other tornado climatology studies showed similar results of a maximized tornado threat somewhere in the Great Plains (e.g., Schaefer et al. 1980). Concannon et al. (2000) and Brooks et al. (2003) utilized tornado days, defined as a day with one or more tornadoes occurring in a 24-h period, rather than tornado totals, to reduce the effects of secular (non-meteorological) changes in tornado reporting over the years. Concannon et al. (2000) found an L-shaped region of maximized significant (F/EF2 or greater) tornado risk, stretching from Alabama to central Oklahoma and then curving back north and east to Iowa. Brooks et al. (2003) included weak (F/EF0 and F/EF1) tornadoes and found a large risk area covering much of the Great Plains and Southeast, including maxima in eastern Colorado and Florida. After the risk area was reduced to include only where there was a predictable tornado season [defined by Brooks et al. (2003) as the trimmed standard deviation in the timing of the peak threat of less than 20 days], the tornado risk area resembled earlier studies, depicting only the Great Plains from northern Texas to North Dakota as a tornado risk area (Dixon et al. 2011).

However, portraying only PTA as a region of elevated tornado risk based upon spring tornado frequency provides an incomplete assessment. While PTA experiences one season of high tornado risk, STA experiences a longer-lasting tornado risk with lower-frequency peaks that are spread out over the year. Gagan et al. (2010), using SPC tornado data (1950–2007), found while PTA significant tornado frequency peaks in May, STA experiences two lesser significant tornado frequency peaks in the months of April and November, while also experiencing a greater frequency of significant nocturnal (0300 UTC to 1000 UTC) tornadoes. The same study also found STA experienced nearly two-thirds (64%) of their tornado-related fatalities in the months October through March, while 88% of PTA tornado-related fatalities occurred in the months April to June. It must be noted there are differences in how STA and PTA are defined in this study and Gagan et al. (2010) (see Sect. 2.1).

It is well known that tornado outbreak events are typically associated with veering wind profiles (e.g., Johns and Doswell 1992) and the quasi-geostrophic (QG) circulation of jet

streams. Due to the proximity of the PTA events to the Rockies, the tendency of wave disturbances to develop lee-side troughing, and the tendency for the STJ to arch poleward toward eastern North America, *we hypothesize that PTA events are most often associated with the QG circulation associated with the PJ*. In contrast, the STA outbreaks are often located where the STJ arches poleward, often in a region where the PJ is also driving poleward. Therefore, *we hypothesize that STA outbreaks are more likely than PTA outbreaks to be associated with a STJ, also likely interacting with a polar jet*. The main goal in this study will be to statistically determine what jet streak types are associated with tornado outbreaks in PTA and STA and evaluate the positioning of jet streak types relative to tornado outbreaks in order to examine these hypotheses.

2 Methodology

2.1 Tornado data and delineation of PTA and STA boundaries

Tornado data used in this study were obtained from the SPC tornado database (SPC 2015a) and SPC Online SeverePlot 3.0 (SPC 2015b), which provide the date, time, intensity (F/EF-Scale rating), touchdown point, path length, path width, fatalities, injuries, among other statistics for all observed tornadoes in the USA from 1950 to 2016. For this study, tornado data for the 30-year period from 1984 to 2013 were used to find tornado outbreaks. The most recent available 30-year period was selected in order to represent a typical climate mean.

Figure 1a depicts the boundaries of the two alleys and all significant tornadoes between 1984 and 2013. The boundaries are based upon a combination of significant and violent tornado frequency and distinguishing characteristics of the alleys. PTA is characterized by sloping terrain, while STA is characterized by its proximity to the Gulf of Mexico. Topography between the two alleys differs; STA generally is lower in elevation, has more rugged and hilly terrain, and has more vegetation than PTA. The more variable terrain in STA may cause a number of effects on tornadogenesis and tornado tracking that differs
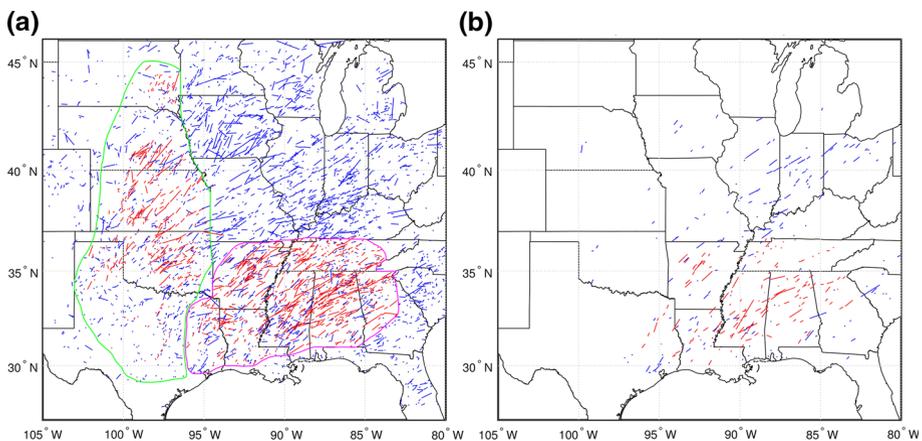

Fig. 1 **a** The boundaries of PTA (green outline) and STA (magenta outline) are shown. Significant tornado tracks are highlighted in blue, while tracks involved in a PTA or STA outbreak are highlighted in red. **b** Same as Fig. 3a, except depicting only November significant tornadoes from 1984 to 2013

from the flat terrain of PTA, but because the understanding of how terrain and vegetation affect tornadogenesis and maintenance remains poorly understood, it will be neglected here. While there was an attempt to only include areas of higher significant or violent tornado frequency, central Texas is the only exception to the rule. The influence this has on the overall results is tiny, as only a few tornadoes from central Texas were included in outbreaks. In general, PTA experiences a maximum peak of significant tornadoes in May, and STA experiences a more annually spread-out tornado season with separate peaks in April and November (Gagan et al. 2010). The distinguishing feature chosen to separate the alleys is the frequency of significant tornadoes during the month of November (Fig. 1b). STA experiences a secondary peak of significant tornadoes during November, while during this time PTA significant tornadoes are rare. The method of outlining the boundaries for both the PTA and STA calls into question whether such sharp, rigid boundaries are appropriate, especially in eastern Texas and Arkansas where the two alleys begin to converge. After all, in terms of tornado frequency there may not be two distinct alleys (Dixon et al. 2011). Yet, for the purposes of this study, in which the goal is to compare two separate regions of higher tornado risk, the assumption will be made they are separate.

As with most climatological studies of elevated tornado risk, there is a fluctuation of regions based upon the parameters chosen to characterize the tornado risk (e.g., path length, width, F/EF-Scale, tornado days). As a result, characterizing any bounded region as a place with greater tornado risk will always have some degree of subjectivity. This certainly holds true for this study, which describes tornado risk by the intensity (F/EF-Scale), path length, and frequency of tornadoes in a region. Still, the regions highlighted to represent PTA and STA correspond well with those in Gagan et al. (2010). Differences among the boundaries between this study and Gagan et al. (2010) include the northern and western extent of PTA, as well as the eastern and western extent of STA. This is mainly due to Gagan et al. (2010) having a strong adherence to state boundaries. A shortcoming of strictly adhering to state boundaries, besides having no physical meteorological significance, is including a greater area of lower tornado risk in an overall region that should be characterized by higher tornado risk.

2.2 Definition of a tornado outbreak

In this study, a case considered a tornado outbreak must have at least one of the following occur within a 24-h time frame in STA or PTA (Fig. 1a):

1. five or more significant (F2/EF2 or greater) tornadoes,
2. two or more violent (F4/EF4 or F5/EF5 rating) tornadoes,
3. total path length of significant tornadoes exceeding 93 mi.

In addition, the tornadoes included in an outbreak must be associated with the same synoptic scale weather system. These criteria were empirically selected with the goal of including only significant tornado outbreaks in the delineated regions, which was earlier described as considering intensity, path length, and frequency of tornadoes. The duration of tornado production, known as the time between the first tornado touchdown and the last tornado touchdown, can exceed 24 h for an ongoing outbreak (e.g., the 27 April 2011 and 15 November 1987 outbreaks), but it does not exceed 30 h; only in five outbreak cases does it exceed 24 h. In total, three outbreaks involved a hurricane making landfall: Hurricane Danny on 15 August 1985, Hurricane Katrina on 29 August 2005, and Hurricane Rita on 24 September 2005. These were excluded from the dataset as hurricane-spawned

tornadoes are unrelated to upper-level jet streaks. There was no distinction made between mesocyclonic tornadoes and non-mesocylonic tornadoes.

2.3 Assessing tornado outbreak intensity

An equitable measure of the intensity of tornado outbreaks is needed to accurately portray tornado risk. For example, selecting the total path length of an outbreak would not be an accurate portrayal of tornado outbreak intensity; an outbreak with two 50-mi-long EF2 tracks is not equivalent in intensity to an outbreak with two 50-mi-long EF4 tracks. However, given a large enough outbreak sample size, and given the rarity of violent tornadoes, this effect becomes much less pronounced. Still, to more accurately depict the tornado risk associated with individual outbreaks, Fujita miles and adjusted Fujita miles (AFMs) were adopted from Furhmann et al. (2014) as a method of assessing tornado outbreak intensity. Fujita miles are calculated simply by multiplying a tornado's path length by its maximum F/EF-Scale rating; AFMs are calculated by multiplying a tornado's path length by an empirically derived scaling factor (Table 1, from Furhmann et al. 2014). The inclusion of an empirically derived scaling factor in the calculation of AFMs takes into account the variability of tornado intensity along its path length. However, this also introduces additional statistical uncertainty into the calculation of AFMs. Of course, other tornado (outbreak) intensity schemes have been created [e.g., the destructive potential index (DPI) developed by Thompson and Vescio (1998), the Forbes impact index by Forbes (2006), and the O index by Doswell et al. (2006)]. One problem with such indices, addressed by Furhmann et al. (2014), is the use of path width, which falls into two different categories in the SPC tornado database. Prior to 1995, path width was reported as the mean tornado path width. Since 1995, the NWS, in consultation with the severe weather community, has decided to record the maximum tornado path width instead, analogous to recording the maximum F/EF-Scale rating along the path of the tornado (although they may not necessarily occur at the same location). As such, Fujita miles and AFMs, which do not use path width, are measurements not prone to error caused by the difference in reporting tornado path width. Fujita miles and AFMs, however, are limited by the uncertainty in F/EF-Scale ratings (e.g., Kelly et al. 1978; Doswell and Burgess 1988; Edwards et al. 2013). If not for the approximations, biases, and errors inherent in tornado data, Fujita miles would be a measurement with a physical foundation; the work done by a tornado is represented by an estimate of tornado force (F/EF-Scale rating) multiplied by distance (path length).

Table 1 Mean adjusted F/EF-Scale ratings with standard deviation and sample size of tornadoes used to calculate the adjusted ratings from Furhmann et al. (2014)

F/EF-Scale rating	Mean adjusted F/EF-Scale rating	SD ($\pm$ 1)	Sample size
1	0.981	0.912–1.050	60
2	1.818	1.456–2.180	32
3	2.769	2.514–3.024	31
4	3.544	3.064–4.024	26
5	4.430	3.830–5.030	4

2.4 Jet identification scheme

The upper-level jet identification scheme used to objectively identify STJs and PJs is adopted from Christenson et al. (2017) and Winters and Martin (2014), which was created using NCEP/NCAR Reanalysis 1 data (Kalnay et al. 1996). In this scheme, first the integrated wind speed is calculated for the 400–100-hPa layer. This is done by computing the horizontal wind speed at every grid point between 400 and 100 hPa, and then vertically averaging every horizontal wind speed between these two levels. Thus, the integrated wind speed is defined by the following equation from Koch et al. (2006):

$$\alpha vel = \frac{1}{p_2 - p_1} \int_{p_1}^{p_2} (u^2 + v^2)^{1/2} dp, \tag{1}$$

where αvel is the scalar quantity representing the integrated wind speed, u and v are, respectively, the zonal and meridional wind components, and the two pressure levels p_1 and p_2 are 100 and 400 hPa, respectively. The scheme then uses potential vorticity and temperature characteristics of the STJ and PJ to identify them within a grid column. A STJ is identified in a grid column where within the 340–355 K layer, a $|\nabla PV|$ threshold of 0.64×10^{-5} PVU m^{-1} is equaled or exceeded within the 1–3-PVU (1 PVU = K m^2 kg^{-1} s^{-1}) channel, and the integrated wind speed in the 400–100-hPa layer is greater than 30 m s^{-1}. The same criteria are used to identify a PJ in a grid column, except using a 315–330 K temperature layer. A superposed jet is identified if the criteria for both the STJ and PJ are met in a single grid column.

Using the jet identification scheme, individual jet streaks were objectively identified as a STJ streak, PJ streak, or superposed jet streak. A jet streak associated with only a STJ identification was labeled as a STJ streak. This was similarly done for PJ identifications and superposed identifications, although it was common for STJ and PJ identifications to be surrounding a superposed identification. For the cases in which both STJ and PJ identifications were considered to be associated with the same jet streak, but there was no superposed identification, a more subjective identification named "merged jet" was created. A "merged jet" is physically distinguished from a superposed jet in that the two jets that have not become superposed (i.e., a three-step tropopause exists rather than the two-step tropopause associated with a superposition event). Figure 2 highlights the jet identifications for a merged jet streak case (left) and a superposed jet streak case (right). In cases where wind maxima greater than 30 m s^{-1} were identified at 200, 250, or 300 hPa using NCEP/NCAR Reanalysis 1 data, but did not meet the criteria to be objectively defined as either a STJ, PJ, or superposed jet streak, the wind maxima were labeled as an "unidentified jet streak." An effort was made to not include jet streaks generated by convective outflow no matter what their identification type was.

In order to describe the tornado outbreak cases based on the types of jet streaks associated with them, four outbreak types were created as follows: STJ and PJ, STJ, PJ, and "no identifications." A STJ and PJ tornado outbreak is defined as any outbreak with separate STJ and PJ streaks, or a merged jet streak, or a superposed jet streak. A STJ (PJ) tornado outbreak is any outbreak associated with a STJ (PJ) streak, but no PJ (STJ) streak. A "no identifications (IDs)" type was created to describe an outbreak associated with only unidentified jet streak(s). Since tornado outbreaks often last longer than 6 h for this study, it was possible for the same jet streak in an outbreak to have changing jet identification types. For example, a jet streak at 1200 UTC could be identified as a PJ streak, but
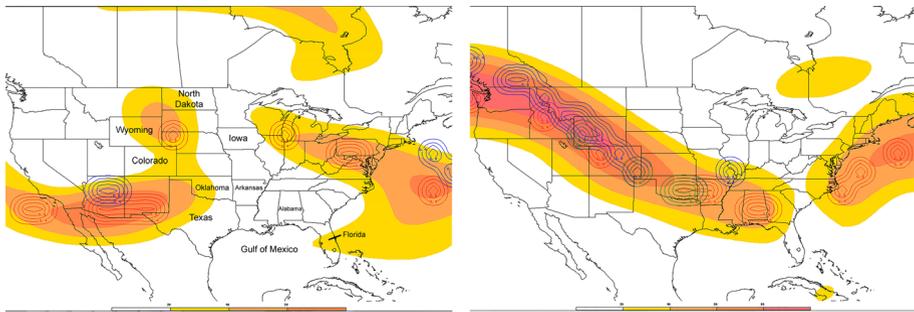
Fig. 2 On the left are the integrated wind speed and jet identifications associated with a PTA STJ and PJ outbreak for a case with a merged jet streak. The same is on the right for an STA STJ and PJ outbreak for a case with a superposed jet streak. Integrated wind speed is shaded every 10 m s^{-1} starting at 30 m s^{-1}. Solid red contours represent STJ identifications, solid blue contours represent PJ identifications, and solid green contours represent superposed identifications. On the right, the superposed identifications are located over Oklahoma, southeastern Colorado, and western Wyoming

identified as a STJ streak 6 h later. In such a case, and vice versa, the jet streak would be defined as merged.

Further analysis of vertical jet cross sections of 104 outbreaks in this 30-year period from 1984 to 2013 reveals some complications exist with the jet identification scheme used in the study. One consistently notable flaw is the PJ identification disappearing downstream when the PJ arches equatorward and merges with a poleward arching STJ. However, no outbreak cases were found where this influenced the outbreak type. This is mainly because this is a transient problem, and many outbreaks last long enough where another reanalysis time has to be considered when categorizing the outbreak type. Another problem found was identified PJs exhibiting a double jet structure and bounding the tropical tropopause. There were three outbreaks in which this may have changed the outbreak from being a STJ and PJ outbreak to a PJ outbreak: 4 April 1989, 1 January 1999, and 24 February 2001. Some jet streaks were not identified (for STJ and PJ cases in both regions, 8 unidentified jets were found out of 132 total jet streaks), likely due to having their vertical PV gradient inside the undefined 330–340 K temperature range or an insufficient vertical PV gradient.

2.5 Composite of jet streak maxima relative to tornado outbreak centroid

Tornado track locations were obtained from the SPC tornado database, and jet streak maxima locations were estimated using NCEP/NCAR Reanalysis 1 data at 200, 250, and 300 hPa, taken four times daily at 00:00 UTC, 06:00 UTC, 12:00 UTC, and 18:00 UTC. Tornado track midpoints were calculated as the geographical centroid of the start and end points of a tornado track (see Appendix "Weighted Geographical Centroid and Weighted Average Angle"). From these, the tornado outbreak centroid was calculated from all individual tornado track midpoints in the outbreak using Eqs. (2) through (6). A caveat to this calculation of the tornado outbreak centroid is it is not representative of outbreaks where tornado track midpoints are concentrated in two or more far apart regions. In that case, the apparent outbreak centroid can be a distance away from where any tornado actually occurred during the outbreak. Examining the minimum distance between a tornado track and the tornado centroid for each case, 48 of 104 outbreaks (46%) have a minimum distance greater than 40.2 km (25 mi), 12 of 104 outbreaks (12%) have a minimum

distance greater than 80.5 km (50 mi), and 1 of 104 outbreaks (1%) have a minimum distance greater than 160.9 km (100 mi).

Jet streak maxima locations were centered to their respective tornado outbreak centroid for Figs. 4, 5, 6 and 7. A flaw of plotting just the center and angle of a jet streak is the structure and scale of the jet streak is not conveyed. Jet streak maxima were excluded from the outbreak case if at least one tornado was not within 1000 km of its jet axis. As determined by numerical studies, 1000 km is approximately the maximum distance from the jet axis where the transverse circulation associated with the jet streak extends (e.g., Keyser and Pecnick 1985; Moore and Vanknowe 1992). The jet axis endpoints are defined as the location where the jet axis intersects the 30 m s^{-1} contour at the level where the local maximum wind speed is estimated (200, 250, or 300 hPa).

Many outbreaks lasting longer than 6 h deal with progressive jet streaks. To avoid the clutter that would be associated with plotting the same jet streak maxima more than once due to its shift in location during the outbreak, the weighted geographical centroid of the jet streak maxima was used to represent the average of the different jet streak positions at different times. This was done by correlating the tornado touchdown times with the closest reanalysis time (0000 UTC, 0600 UTC, 1200 UTC, or 1800 UTC) in order to calculate a weighting for the reanalysis time's jet streak maxima position. In other words, the significant tornado AFMs from 2100 UTC to 0259 UTC were correlated to the 0000 UTC reanalysis, AFMs from 0300 UTC to 0859 UTC were correlated to the 0600 UTC reanalysis, AFMs from 0900 UTC to 1459 UTC were correlated to the 1200 UTC reanalysis, and AFMs from 1500 UTC to 2059 UTC were correlated to the 1800 UTC reanalysis. The weighting for a jet streak at a certain reanalysis time is calculated by adding all significant tornado AFMs correlated to the same reanalysis time and dividing by the cumulative AFMs of the outbreak. The reasoning of why the individual jet maxima positions were weighted by cumulative significant tornado AFMs was in order to better represent the location of the jet streak when the outbreak was producing more AFMs.

3 Results and discussion

A complete tabular listing of cases and their statistic attributes are found in Online Resource 1. During the 30-year period from 1984 to 2013, 65 tornado outbreaks were recorded in STA and 39 outbreaks were recorded in PTA for a total of 104 outbreaks in the two alleys. A breakdown of outbreak types is summarized in Table 2. The findings show STJ and PJ outbreaks composed the majority of outbreaks in PTA and STA. Notably, STJ

Table 2 Number and percentage of tornado outbreaks by outbreak type in PTA and STA

PTA		STA	
Outbreak classification	Number of outbreaks	Outbreak classification	Number of outbreaks
STJ and PJ	20 (51%)	STJ and PJ	45 (69%)
STJ	11 (28%)	STJ	5 (8%)
PJ	1 (3%)	PJ	12 (18%)
No IDs	7 (18%)	No IDs	3 (5%)
Total	39	Total	65

outbreaks were more common in PTA than in STA, while PJ outbreaks were more common in STA than in PTA. Thus, the initial hypothesis that the PJ was going to play a more important role in PTA has been proven false. Instead, it is found a PJ is more likely to be associated with a STA outbreak than with a PTA outbreak. Such results show preconceived notion does not always match reality. The second hypothesis that a STJ interacting with a PJ was more likely in STA outbreak than in PTA outbreaks has been confirmed, although the majority of PTA outbreaks are STJ and PJ outbreaks.

Considering only jet streak types (e.g., STJ, PJ, merged, and superposed), tornado outbreaks in PTA (21 of 39 cases or 54%) were more likely to be associated with a STJ streak than tornado outbreaks in STA (25 of 65 cases or 38%). A tornado outbreak associated with a PJ streak was less common in PTA (9 of 39 cases or 23%) than in STA (26 of 65 cases or 40%). The same is true for merged jets streaks, with 14 of 39 outbreaks (36%) associated with merged jets in PTA and 33 of 65 outbreaks (51%) in STA. When merged jet streaks are not considered a jet type, but instead separate STJ streaks and PJ streaks, then 31 of 39 (79%) of PTA outbreaks and 50 of 65 (77%) of STA outbreaks are associated with STJ streaks, while 21 of 39 (54%) of PTA outbreaks and 57 of 65 (88%) of STA outbreaks are associated with PJ streaks. The main theme in all of these results is the PJ is less frequent in PTA outbreaks, which results in fewer tornado outbreaks where the STJ and PJ more closely interact to form merged jet streaks.

STJ and PJ tornado outbreaks are more frequent in PTA and STA, but the strength of these outbreaks is still in question. To compare the strength of tornado outbreaks associated with different jet types, significant tornado AFMs were utilized. Figure 3 shows the comparison of the cumulative significant AFMs of STJ and PJ outbreaks to all other outbreaks for PTA and STA. The 27 April 2011 outbreak is plotted in Fig. 3, but it is not visibly displayed since it is too much of an outlier; displaying it compromises the overall visual presentation. In PTA, STJ and PJ outbreaks are clearly on average stronger than other outbreaks. There is less of a difference between STJ and PJ outbreaks and other
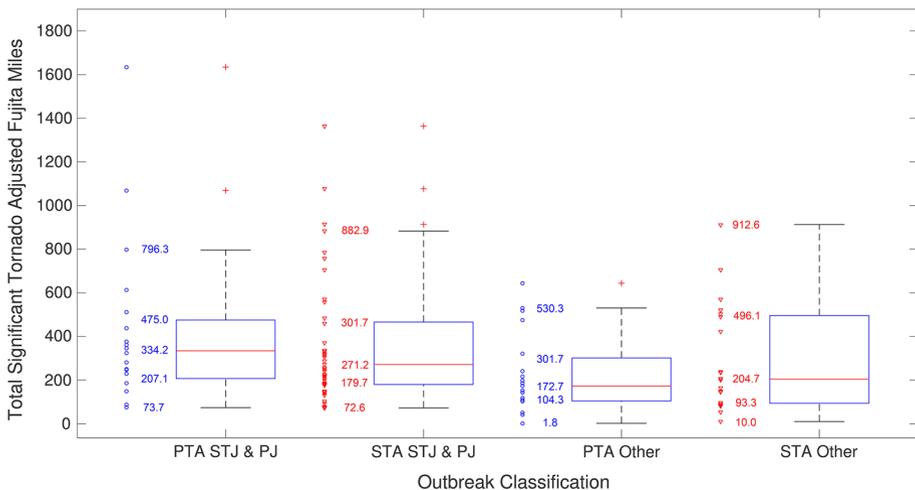

Fig. 3 A box plot chart and vertical scatter plot (left of box plot) comparing cumulative significant tornado AFMs for STJ and PJ outbreaks versus all other outbreaks for PTA and STA. Blue circles represent PTA outbreaks, while red triangles represent STA outbreaks. The 27 April 2011 outbreak is off-figure for STA STJ and PJ outbreaks

outbreak types in STA in terms of the distribution of cumulative significant tornado AFMs. This suggests while STJ and PJ outbreaks are stronger in STA, it may be to a lesser degree. The clearest discrimination between STJ and PJ outbreaks and other outbreak types in both alleys is the minimum cumulative significant AFMs; in both alleys, the minimum is above 70 AFMs for STJ and PJ outbreaks.

With the frequency and strength of STJ and PJ outbreaks documented in both alleys, the position of jet streaks relative to the outbreak centroid may reveal further insights into what jet streak configurations have a tendency to produce more cumulative significant tornado AFMs in STJ and PJ outbreaks. Figures 4, 5 and 6 depict the spatial distribution of jet streak maxima for STJ and PJ outbreaks in both alleys relative to their corresponding outbreak centroid, while Table 3 gives a detailed breakdown of the figures based on jet type and sector number. The figure for STA is divided into two based on cumulative
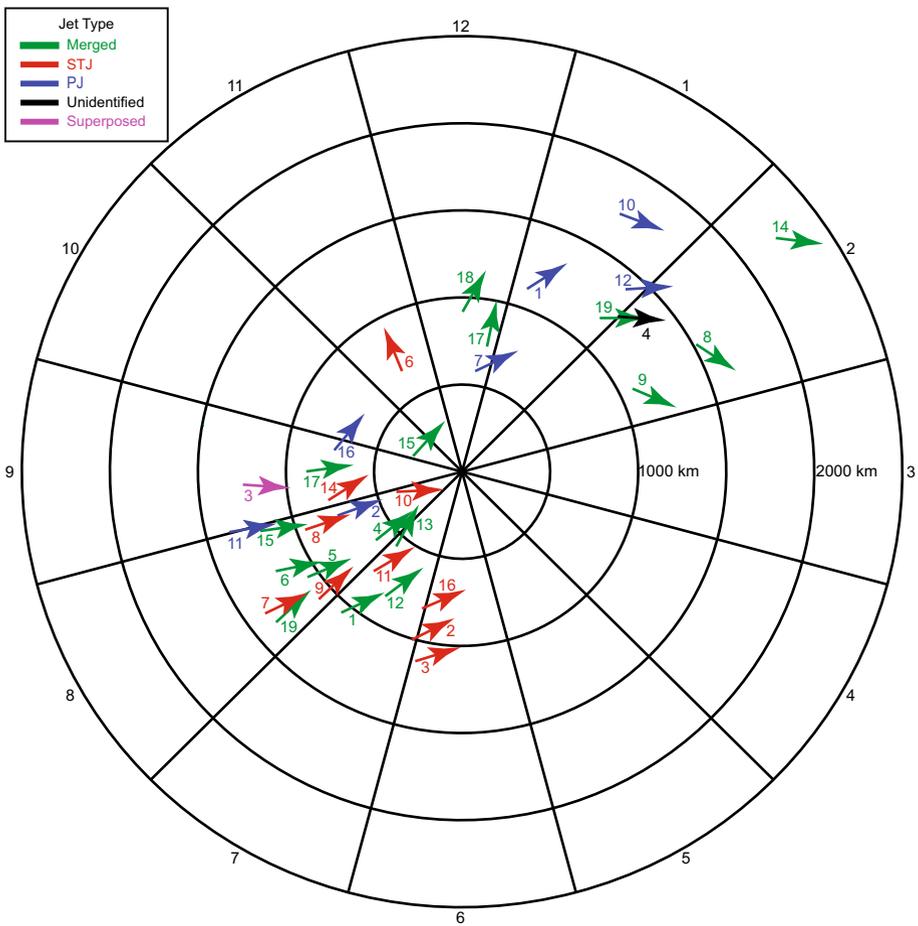

Fig. 4 A composite diagram mapping the approximate headings and locations of jet streak maxima centered relative to each tornado outbreak centroid for PTA STJ and PJ outbreak cases ranked in descending order by significant tornado AFMs. Vectors representing jet streak maxima locations are labeled by their outbreak rank and are colored according to jet type: STJ (red), PJ (blue), merged (green), and unidentified jet (black). Every sector is labeled 1–12
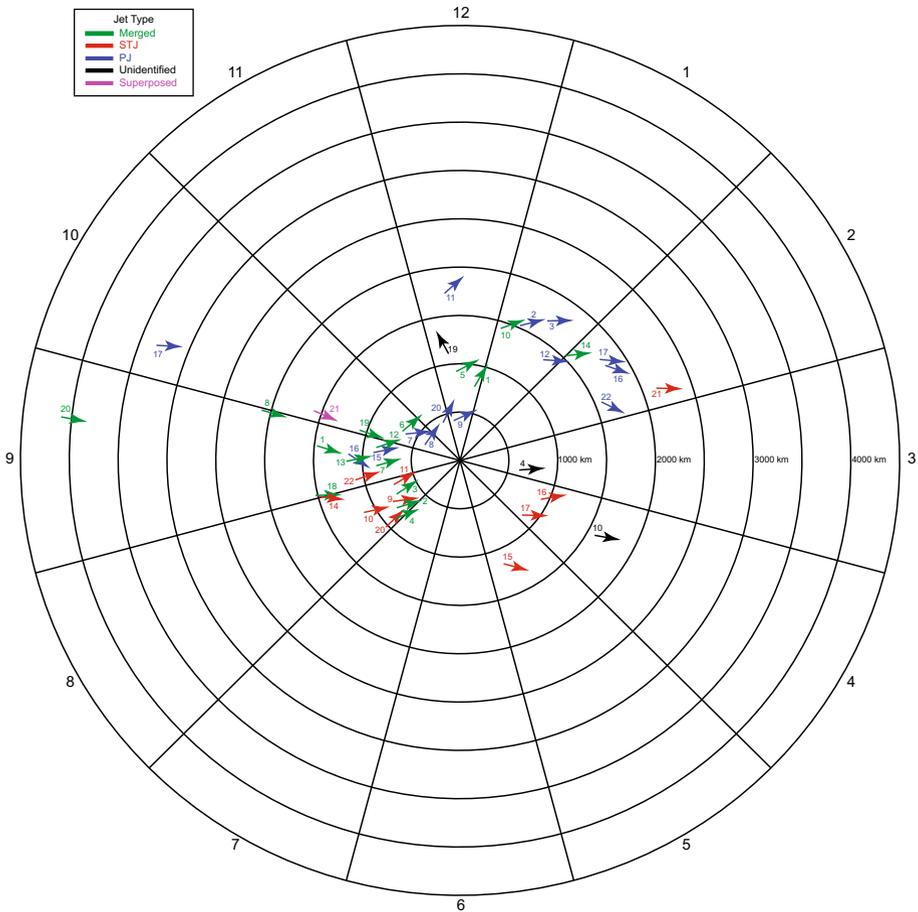
Fig. 5 Same as Fig. 4, except plotting the top 50% of STA STJ and PJ outbreaks in terms of significant tornado AFMs. Vectors are colored according to jet type: STJ (red), PJ (blue), merged (green), unidentified jet (black), and superposed jet (magenta). Every sector is labeled 1–12

significant tornado AFMs, with one depicting the top 50% of outbreaks ranked by cumulative significant tornado AFMs, and the other the bottom 50%. This is done so the sample sizes of jet streaks are more comparable between alleys; it also results in a comparison of jet type and position between higher- and lower-end STA STJ and PJ outbreaks. In lower-end STA STJ and PJ outbreaks, sectors 8–12 and 1 (225° to 45° clockwise) contain the vast majority of jet streaks (39 out of 44); in higher-end STA STJ and PJ outbreaks, the same sectors contain an overwhelming majority of jet streaks (33 out of 44); in PTA, the majority of jet streaks are in these sectors (22 out of 35). This suggests if you draw a 45° tilted line through the centroid of an outbreak, most of the jet streaks influencing the outbreak will be on the left side of the line, especially in STA outbreaks. No jet streaks in PTA STJ and PJ outbreaks were found to approach from the northwest, while 13 such cases in STA STJ and PJ outbreaks were found. A jet streak approaching from the northwest in PTA would have a transverse circulation with a return flow resulting in the advection of warm, dry air at low levels from more arid regions (e.g., the Mexican
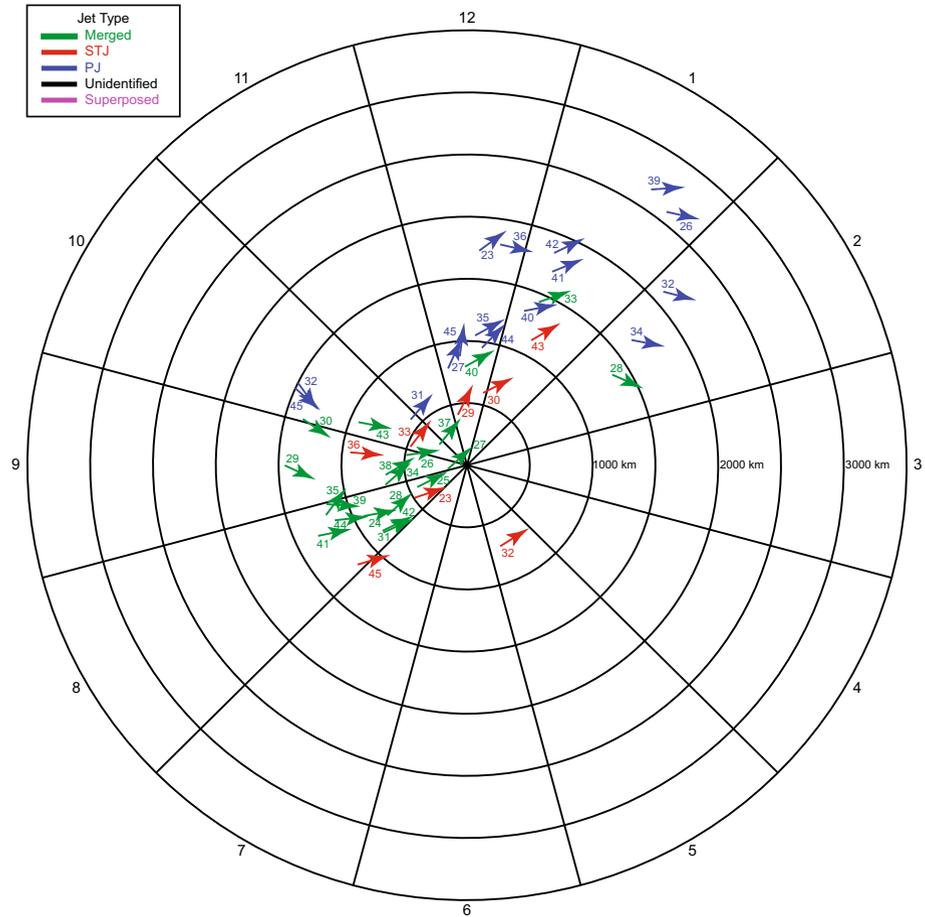
Fig. 6 Same as Fig. 5, but instead the bottom 50% of STA STJ and PJ outbreaks are plotted in terms of significant tornado AFMs

Plateau). This may result in too strong of an elevated mixed layer to support a regional outbreak of significant tornadoes. The majority of merged jet streaks in STA are located in sectors 8–10, while the majority of merged jet streaks in PTA are located in sectors 7 and 8. There appears to be no correlation between merged jet streaks and outbreak strength in either alley, although merged jet streaks are somewhat less frequent in higher-end STA STJ and PJ outbreaks. In lower-end STA STJ and PJ outbreaks, the majority of PJ streaks are located in sectors 1 and 2 (15° to 45°).

A notable trend is discerned in both alleys; outbreaks involving a STJ/merged jet streak arching poleward from sector 8 (225° to 255°) generally had more cumulative significant tornado AFMs (Figs. 4, 5, 6). These outbreaks were also associated with a PJ streak or merged jet streak upstream to the northeast. This structure closely resembles the coupled jet structure identified in other studies, where the divergence aloft from the cyclonic exit region of one jet streak and the anticyclonic entrance region of another jet streak are co-

Table 3 Table based on Figs. 4, 5 and 6 showing the count of each jet type for sectors 1 through 12 for the PTA and STA STJ and PJ outbreaks. Outbreaks in both alleys are divided in half based on cumulative significant tornado AFM rankings. Values of zero are left blank

Outbreak type	Sector number	STJ	PJ	Merged	Superposed	No IDs	Total
PTA STJ and PJ	1		3				3 (9%)
	2		1	4		1	6 (17%)
	6	3					3 (9%)
	7	1		3			4 (11%)
	8	4	2	5			11 (31%)
	9	1		1	1		3 (9%)
	10		1				1 (3%)
	11	1		1			2 (6%)
	12			2			2 (6%)
	All	10 (29%)	7 (20%)	16 (46%)	1 (3%)	1 (3%)	35
STA STJ and PJ	1		3	1			4 (9%)
(top 50%)	2	1	3	1			5 (11%)
	3					1	1 (2%)
	4	2				1	3 (7%)
	5	1					1 (2%)
	7			1			1 (2%)
	8	5		2			7 (16%)
	9	1	2	7			10 (23%)
	10		3	2	1		6 (14%)
	12		3	2		1	6 (14%)
	All	10 (23%)	14 (32%)	16 (36%)	1 (2%)	3 (7%)	44
STA STJ and PJ	1	2	5	1			8 (18%)
(bottom 50%)	2		2	1			3 (7%)
	5	1					1 (2%)
	7	1					1 (2%)
	8	1		9			10 (23%)
	9	1		4			5 (11%)
	10	1	2	2			5 (11%)
	11		1	2			3 (7%)
	12	1	6	1			8 (18%)
	All	8 (18%)	16 (36%)	20 (45%)			44

located and result in a region of enhanced large-scale ascent (e.g., Hakim and Uccellini 1992). Coupled jet structures are more common in STA than in PTA. Figure 7a depicts the jet streak maxima and tornado tracks of the top 5 strongest STJ and PJ outbreaks in this study. Two of these outbreaks perfectly matched the described trend, while one very nearly matched the trend with a STJ instead located in sector 7. The 27 April 2011 outbreak, however, did not match this trend, and its tornado tracks over-represent the figure.
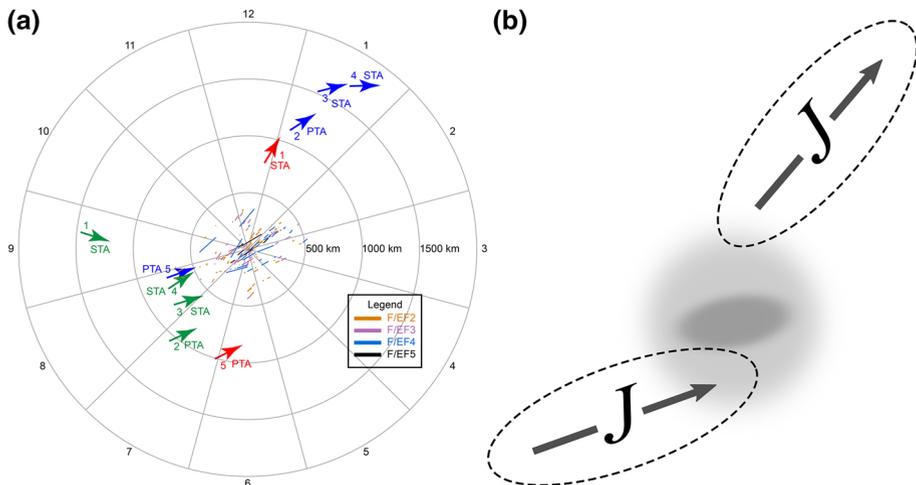
Fig. 7 a A composite diagram of tornado tracks and jet streak maxima position and bearing relative to tornado outbreak centroid for the top five strongest STJ and PJ outbreaks in terms of cumulative significant tornado AFMs. Vectors representing jet streak maxima locations are labeled by their AFM rank and tornado alley. Vectors are colored according to jet streak type: STJ (red), PJ (blue), merged jet (green), and unidentified jet (black). Sectors are labeled 1–12. Tornado tracks are colored according to F/EF-Scale in the legend shown. **b** A conceptual model diagram depicting the coupled jet streak structure associated with three of the top five strongest STJ and PJ outbreaks in terms of cumulative significant tornado AFMs. The light-shaded region represents roughly the area of greatest significant tornado potential, while the dark-shaded region is where violent tornadoes are most favorable

4 Conclusions

The importance of the STJ streak to tornado outbreaks, together with the involvement of the PJ streak, is suggested by the results; this study concludes that STJ and PJ outbreaks compose the majority of tornado outbreaks and that these tornado outbreaks are stronger on average. Also apparent is how outbreak regions have their own characteristics in terms of outbreak type frequency; STJ outbreaks are more common in the Plains than in the Southeast, while PJ outbreaks are more common in the Southeast. However, in both of these regions, tornado outbreaks with jet streaks approaching from the southwest to west-southwest, coupled with a jet streak to the northeast, have been found to be correlated with stronger tornado outbreaks.

Importantly, our initial hypothesis that PTA events are most often associated with the QG circulation associated with the PJ has been rejected. A PJ is more likely to be associated with a STA outbreak than a PTA outbreak. And although our hypothesis that STA outbreaks are more likely than PTA outbreaks to be associated with a STJ, also likely interacting with a polar jet, has been accepted by our results, what is apparent is both our hypotheses underestimated the frequency of the STJ in PTA outbreaks. This suggests the STJ is important to tornado outbreaks given their high frequency in tornado outbreaks in both PTA and STA. This suggests the STJ is important to tornado outbreaks given their high frequency in tornado outbreaks in both PTA and STA. Important to the stronger tornado outbreaks is the interaction of STJ and PJ streaks, especially in the coupled jet structure earlier identified.
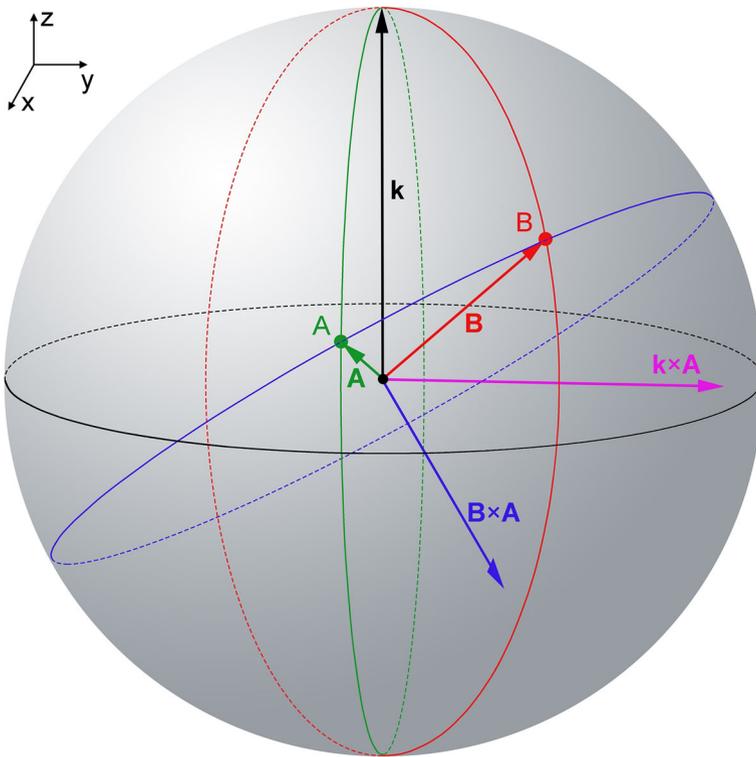
Fig. 8 A geometric figure to aid the description of how great-circle distance and initial bearing is calculated, which is used in plotting Figs. 4, 5, 6 and 7

Exactly why the coupled jet structure is correlated with stronger tornado outbreaks should be a goal of future research, but speculation is briefly presented here. Observation finds the strongest STJ and PJ outbreaks (three of the top five strongest in terms of AFMs) are influenced by the left jet exit region of a merged jet streak or STJ streak and the right jet entrance region of a PJ streak (Fig. 7b). In this manner, the ageostrophic transverse circulations align to create enhanced large-scale ascent between the two jet streaks, which are also partly responsible for enhanced warm air advection and low-level moisture advection underneath the STJ streak. Warm air advection increases the veering wind profile of the atmosphere. It is surmised the way in which the two jets interact creates unidirectional winds aloft, with veering winds occurring primarily only in the lowest 0 to 6 km layer above ground. This is more favorable for supercell tornado development compared to winds veering aloft, which is found closer to the right-entrance region of the PJ streak. Figure 7b, which depicts an idealized STJ and PJ outbreak, highlights that significant and violent tornadoes are more probable closer to the poleward arching STJ or merged jet. We hypothesize the way in which the two jets come together creates a three-dimensional wind field with large values of helicity. The aligned vertical transverse circulations cause a higher rate of mass evacuation or negative surface pressure tendency; this increases the isallobaric component of the ageostrophic wind that forms the low-level jet (Uccellini and Johnson 1979). Thus, a stronger low-level jet may be associated with a coupled jet structure, which creates a low-level wind profile more favorable for tornado

occurrence. However, modeling and analyzing this hypothesis is beyond the scope of this study.

Appendix

Weighted geographical centroid and weighted average angle

To create the plots in Figs. 4, 5, 6 and 7, calculations for average position and average angle were necessary. To represent average position, the geographical centroid between two or more points on earth were calculated under the assumption the earth is a perfect sphere. Taking the latitude and longitude of point n, one can convert to Cartesian coordinates and find the weighted average of the x, y, and z coordinates via the following:

$$x_{\text{avg}} = \frac{\sum_{k=1}^{n} [R_{\text{E}} \cos(lat_n) \cos(lon_n)w_n]}{\sum_{k=1}^{n} w_n}, \tag{2}$$

$$y_{\text{avg}} = \frac{\sum_{k=1}^{n} [R_{\text{E}} \cos(lat_n) \sin(lon_n)w_n]}{\sum_{k=1}^{n} w_n}, \tag{3}$$

$$z_{\text{avg}} = \frac{\sum_{k=1}^{n} [R_{\text{E}} \sin(lat_n)w_n]}{\sum_{k=1}^{n} w_n}, \tag{4}$$

where x_{avg}, y_{avg}, and z_{avg} are the weighted averages of the x, y, and z coordinates, lat_n is the latitude of point n in radians, lon_n is the longitude of point n in radians, R_{E} is the radius of the earth, and w_n is a weighting. If there is equal weighting between points, the weighting is equal to 1. The value of R_{E} is not important for the next calculation as long as it is positive and nonzero, and may be omitted. To convert from Cartesian coordinates back to spherical coordinates, the atan2(y, x) function is used:

$$lat_{\text{cent}} = \text{atan2}(z_{\text{avg}}, \sqrt{x_{\text{avg}}^2 + y_{\text{avg}}^2}) \cdot \frac{180}{\pi}, \tag{5}$$

$$lon_{\text{cent}} = \text{atan2}(y_{\text{avg}}, z_{\text{avg}}) \cdot \frac{180}{\pi}, \tag{6}$$

where lat_{cent} and lon_{cent} are the latitude and longitude of the geographical centroid in degrees and the two-argument atan2 function uses the signs of both arguments in order to place the angle in the appropriate quadrant. While the atan2 function has a range of $(-\pi, \pi]$, the one-argument arctangent function has a limited range of $(-\pi/2, \pi/2)$ and thus cannot make a distinction between opposite angles such as $\pi/4$ and $3\pi/4$.

The weighted average angle θ_{avg} in degrees was also calculated for two or more angles θ_n in radians using the atan2 function as follows:

$$\theta_{avg} = \text{atan2}\left(\sum_{k=1}^{n} [\sin(\theta_n)w_n], \sum_{k=1}^{n} [\cos(\theta_n)w_n]\right) \cdot \frac{180}{\pi}, \qquad (7)$$

where w_n is a weighting. This formula is the result of converting each angle θ_n from polar to Cartesian coordinates, performing a weighted average of the Cartesian components of each point, and then converting back to polar coordinates. One may notice both the summation of weighted x and y components should be divided by n to calculate the actual weighted mean, but this has been omitted for the same reason R_E is able to be omitted in (2), (3), and (4); if the scaling of both arguments for the atan2 function is equal, it has no influence on the final result.

Plotting geographical coordinates on a Cartesian grid

To plot the location of each jet streak maximum on a Cartesian grid for Figs. 4, 5, 6 and 7, the geographical coordinates of the jet streaks were converted to polar coordinates, then to Cartesian coordinates, and scaled appropriately. To get to polar coordinates, the distance and angle between the outbreak centroid and jet streak maxima were calculated. Since the earth is assumed to be a perfect spear, the shortest distance between two points on a sphere must be calculated, known as the great-circle distance. To calculate the great-circle distance between the outbreak centroid and jet streak maxima, consider two points A and B on the surface of a sphere (Fig. 8). The blue arc between points A and B represents the great-circle distance. Without simplification, unit vector **A** can be expressed as $(\cos(lat1)\cos(lon1), \sin(lat1)\cos(lon1), \sin(lat1))$ in Cartesian coordinates, and unit vector **B** can be expressed similarly in terms of $lat2$ and $lon2$. The central angle α between unit vectors **A** and **B** can be found by the dot product of these vectors: $\cos(\alpha) = \vec{A} \cdot \vec{B}$ $= \cos(lat1)\cos(lat2)[\cos(lon1)\cos(lon2) + \sin(lon1)\sin(lon2)] + \sin(lat1)\sin(lat2)$ $= \cos(lat1)\cos(lat2)\cos(lon1 - lon2) + \sin(lat1)\sin(lat2)$. Thus, the great-circle distance is

$$D = R \times \arccos(\sin(lat1)\sin(lat2) + \cos(lat1)\cos(lat2)\cos(lon1 - lon2), \qquad (8)$$

where D is the great-circle distance in km, R is an estimate of earth's ellipsoidal quadratic mean radius (6373 km), $lat1$ and $lon1$ are the latitude and longitude of the jet streak maximum converted from degrees to radians, and $lat2$ and $lon2$ are the latitude and longitude of the respective tornado outbreak centroid converted from degrees to radians.

Due to the angle or bearing changing along the path of a great circle, the final bearing will differ from the initial bearing. To calculate the average bearing, first the initial bearing was calculated as:

$$\varphi_i = \text{mod}\left(\text{atan2}(y, x) \cdot \frac{180}{\pi}, 360\right), \qquad (9)$$

where φ_i is the initial bearing, $y = \cos(lat2)\sin(lon2 - lon1)$, and $x = \cos(lat1)\sin(lat2) - \sin(lat1)\cos(lat2)\cos(lon2 - lon1)$. The function mod is the usual modulo operation, and the atan2 function is the same as the one previously used in Sect. 2e. To explain the calculation of initial bearing in more detail, consider two points A and B on a unit sphere (Fig. 8). To simplify the derivation, point A has been chosen to have no y-component and its corresponding unit vector **A** can be expressed as $(\cos(lat1), 0, \sin(lat1))$ in Cartesian coordinates; unit vector **B** is $(\cos(lat2)\cos(lon2 - lon1), \cos(lat2)\sin(lon2 - lon1), \sin(lat2))$, and unit vector **k** is

$(0, 0, 1)$ in Cartesian coordinates. The angle between the plane parallel to vectors **A** and **k** (parallel to the green ellipse in Fig. 8) and the plane parallel to vectors **A** and **B** (parallel to the blue ellipse in Fig. 8) is the initial bearing φ_i. Thus, φ_i is also the angle between cross products $\mathbf{k} \times \mathbf{A}$ and $\mathbf{B} \times \mathbf{A}$. With $\mathbf{k} \times \mathbf{A}$ resulting in vector $(0, \cos(lat2), 0)$ and $\mathbf{B} \times \mathbf{A}$ resulting in vector $(\sin(lat1)\cos(lat2)\sin(lon2 - lon1),$ $\cos(lat1)\sin(lat2) - \sin(lat1)\cos(lat2)\cos(lon2 - lon1), -\cos(lat1)\cos(lat2)\sin(lon2 - lon1))$, the tangent of the angle between vectors $\mathbf{k} \times \mathbf{A}$ and $\mathbf{B} \times \mathbf{A}$ is $\frac{\sqrt{[\sin(lat1)\cos(lat2)\sin(lon2 - lon1)]^2 + [-\cos(lat1)\cos(lat2)\sin(lon2 - lon1)]^2}}{\cos(lat1)\sin(lat2) - \sin(lat1)\cos(lat2)\cos(lon2 - lon1)}$. The numerator can be simplified as $\sqrt{\cos^2(lat2)\sin^2(lon2 - lon1)} \cdot \sqrt{\sin^2(lat1) + \cos^2(lat1)}$, which is equal to $\cos(lat1)\sin(lon2 - lon1)$. In (9), arctan2 of this expression was used to calculate the initial bearing, and then the modulo function was used to yield a result between 0° and 360°. To calculate the final bearing φ_f, (9) was used, except $lat1$ and $lon1$ were, respectively, exchanged with $lat2$ and $lon2$, and the angle was reversed by adding 180°. The modulo function $\mod(\varphi_f, 360)$ was used so φ_f would be between 0° and 360°. To get the average bearing, φ_i and φ_f were averaged using (7), and this result was used as the angle between the jet streak maximum and tornado outbreak centroid. To plot on a Cartesian grid, both the calculated great-circle distance and average bearing were used to convert from polar coordinates to Cartesian coordinates, and distance was scaled appropriately.

References

Ashley WS (2007) Spatial and temporal analysis of tornado fatalities in the United States: 1880–2005. Wea Forecast 22:1214–1228

Ashley WS, Krmenec AJ, Schwantes R (2008) Vulnerability due to nocturnal tornadoes. Wea Forecast 23:795–807

Beebe RG, Bates FC (1955) A mechanism for the release of convective instability. Mon Wea Rev 83:1–10

Bluestein HB, Thomas KW (1984) Diagnosis of a jet streak in the vicinity of a severe weather outbreak in the Texas Panhandle. Mon Wea Rev 112:2499–2520

Brooks HE, Doswell CA III, Kay MP (2003) Climatological estimates of local daily tornado probability for the United States. Wea Forecast 18:626–640

Christenson CE, Martin JE, Handlos ZJ (2017) A synoptic-climatology of Northern Hemisphere, cold season polar and subtropical jet superposition events. J Clim 29 (in press)

Clark AJ, Schaffer CJ, Gallus WA Jr, Johnson-O'Mara K (2009) Climatology of storm reports relative to upper-level jet streaks. Wea Forecast 24:1032–1051

Concannon PR, Brooks HE, Doswell CA III (2000) Climatological risk of strong to violent tornadoes in the United States. Preprints, 2nd symposium on environmental applications, Long Beach, CA, Am Meteor Soc, pp 212–219

Dixon PG, Mercer AE, Choi J, Allen JS (2011) Tornado risk analysis: is Dixie Alley an extension of Tornado Alley? Bull Am Meteor Soc 92:433–441

Doswell CA III, Burgess DW (1988) On some issues of United States tornado climatology. Mon Wea Rev 116:495–501

Doswell CA III, Edwards R, Thompson RL, Hart JA, Crosbie KC (2006) A simple and flexible method for ranking severe weather events. Wea Forecast 21:939–951

Edwards R, LaDue JG, Ferree JT, Scharfenberg K, Maier C, Coulbourne WL (2013) Tornado intensity estimation: past, present and future. Bull Am Meteor Soc 94:641–653

Fawbush EJ, Miller RC, Starrett LG (1951) An empirical method of forecasting tornado development. Bull Am Meteor Soc 32:1–9

Forbes GS (2006) Meteorological aspects of high-impact tornado outbreaks. Preprints, Symposium on the Challenges of Severe Convective Storms, Atlanta, GA, Am Meteor Soc, P1.12. https://ams.confex.com/ams/pdfpapers/99383.pdf

Furhmann CM, Konrad CE II, Kovach MM, McLeod JT, Schmitz WG, Dixon PG (2014) Ranking of tornado outbreaks across the United States and their climatological characteristics. Wea Forecast 29:684–701

Gagan JP, Gerard A, Gordon J (2010) A historical and statistical comparison of "Tornado Alley" to "Dixie Alley". Natl Wea Dig 34(2):145–155

Hakim GJ, Uccellini LW (1992) Diagnosing coupled jet-streak circulations for a northern plains snow band from the operational nested-grid model. Wea Forecast 7:26–48

Hales JE (1979) On the relationship of 250 mb positive vorticity advection and horizontal divergence to tornado and severe thunderstorm occurrence. Preprints, 11th Conference on severe local storms, Kansas City, MO, Am Meteor Soc, pp 28–31

Johns RH, Doswell CA (1992) Severe local storms forecasting. Wea. Forecast 7:588–612

Kalnay E et al (1996) The NCEP/NCAR 40-year reanalysis project. Bull Am Meteor Soc 77:437–471

Kelly DL, Schaefer JT, McNulty RP, Doswell CA III, Abbey RF (1978) An augmented tornado climatology. Mon Wea Rev 106:1172–1183

Keyser D, Pecnick MJ (1985) Diagnosis of ageostrophic circulations in a two-dimensional primitive equation model of frontogenesis. J Atmos Sci 42:1283–1305

Koch P, Wernli H, Davies HC (2006) An event-based jet-stream climatology and typology. Int J Climatol 26:283–301

Lee JT, Galway JG (1956) Preliminary report on the relationship between the jet at the 200-mb level and tornado occurrence. Bull Am Meteor Soc 37:327–332

Lee JT, Galway JG (1958) The jet chart. Bull Am Meteor Soc 39:217–223

McNulty RP (1978) On upper tropospheric kinematics and severe weather occurrence. Mon Wea Rev 106:662–672

Moore JT, VanKnowe GE (1992) The effect of jet-streak curvature on kinematic fields. Mon Wea Rev 120:2429–2441

Palmén E, Newton CW (1969) Atmospheric circulation systems. Academic Press, London

Reiter ER (1963) Jet stream meteorology. University of Chicago Press, Chicago, p 515

Riehl H et al (1952) Forecasting in the Middle Latitudes. Am Meteor Soc Mono 5:80

Rose SF, Hobbs PV, Locatelli JD, Stoelinga MT (2004) A 10-yr climatology relating the locations of reported tornadoes to the quadrants of upper-level jet streaks. Wea Forecast 19:301–309

Schaefer JT, Edwards R (1999) The SPC tornado/severe thunderstorm database. Preprints, 11th Conference on applied climatology, Dallas, TX, Am. Meteor. Soc., 6.11. https://ams.confex.com/ams/99annual/abstracts/1360.htm

Schaefer JT, Kelly DL, Doswell CA, Galway JG, Williams RJ, McNulty RP, Lemon LR, Lambert BD (1980) Tornadoes, when, where, how often. Weatherwise 33:52–59

Storm Prediction Center (2015a) Severe Weather Database Files (1950–2014). http://www.spc.noaa.gov/wcm/#data. Accessed 8 Mar 2015

Storm Prediction Center (2015b) SPC Online SeverePlot 3.0. http://www.spc.noaa.gov/climo/online/sp3/plot.php. Accessed 8 Mar 2015

Thompson RL, Vescio MD (1998) The destruction potential index—A method for comparing tornado days. Preprints, 19th Conference on Severe Local Storms, Minneapolis, MN, Am Meteor Soc, pp 280–282

Uccellini L, Johnson D (1979) The coupling of upper and lower tropospheric jet streaks and implications for the development of severe convective storms. Mon Wea Rev 107:682–703

Whitney LF (1977) Relationship of the subtropical jet stream to severe local storms. Mon Wea Rev 105:398–412

Winters AC, Martin JE (2014) The role of a polar/subtropical jet superposition in the May 2010 Nashville Flood. Wea Forecast 29:954–974